J. Fluid Mech. (2004), *vol.* 505, *pp.* 323–347.
DOI: 10.1017/S0022112004008596 Printed in the United Kingdom

Fully nonlinear solitary waves in a layered stratified fluid

By DORIAN FRUCTUS AND JOHN GRUE

Mechanics Division, Department of Mathematics, University of Oslo,
P.O. Box 1053 Blindern, 0316 Oslo, Norway
dorianf@math.uio.no
johng@math.uio.no

(Received 12 February 2003 and in revised form 24 November 2003)

Fully nonlinear solitary waves in a layered stratified fluid, each layer with a constant Brunt–Väisälä frequency, are investigated. The stream function satisfies the Helmholtz equation in each layer and is expressed in terms of singularity distributions. As the Green function, a combination of Bessel functions of order zero, of the second and first kind is advocated. Computations performed for two- and three-layer cases show that the wave speed increases with increasing stratification of the top layer. The thickness of the pycnocline increases with wave amplitude when the top layer is homogeneous but decreases when the top layer is stratified. The wave width depends little on the pycnocline thickness. The fluid velocity may exceed the wave speed in the upper part of the water column when the top layer is stratified, but is always smaller than the wave velocity if the top layer is homogeneous. A large vertical excursion of the individual isopycnals contributes to a small Richardson number Ri. The smallest value of Ri is observed in the main body of the fluid. Solitary waves of increasing strength are investigated until the wave-induced fluid velocity equals the wave speed, or the minimal Ri becomes smaller than one quarter. The results may support experimental studies of breaking internal solitary waves.

1. Introduction

Fully nonlinear interface models are widely used to study internal solitary waves of large amplitude. Besides steady wave theories (Amick & Turner 1986; Turner & Vanden-Broeck 1988; Pullin & Grimshaw 1988; Evans & Ford 1996; Grue *et al.* 1999; Rusås & Grue 2002) unsteady formulations are used to compute the transient formation of the waves (Eliassen & Fjørtoft 1992; Grue *et al.* 1997). Solitary waves in continuously stratified fluids (Tung, Chan & Kubota 1982; Turkington, Eydeland & Wang 1991; Brown & Christie 1998; Grue *et al.* 2000) and unsteady waves (Lamb 1994, 2002) share many of the properties of interfacial waves, but also exhibit particularities that are less understood. The need for fully nonlinear models is motivated by observations of large-amplitude wave motion (Huthnance 1989; Ostrovsky & Stepanyants 1989). Measurements show excursions of the pycnoclines that exceed the thickness of the upper thinner layer of the ocean. Several of the recordings have a wave amplitude that may be four to five times the thickness of the layer above the pycnocline (Stanton & Ostrovsky 1998).

Overturning of internal gravity waves may take place due to convective instability caused by horizontal advection of density. For a single wave this occurs when the horizontal particle velocity exceeds the wave velocity (Orlanski & Bryan 1969;

Delisi & Orlanski 1975). Experimental observations of breaking-induced regions of recirculation (rotors), which transport a core of mixed fluid, have been made (Castro, Snyder & Marsh 1983; Grue *et al.* 2000). Such behaviour is also observed in computations of large solitary waves that break during the process of shoaling (Lamb 2002). Recently, Lamb (2003) studied how a background shear influences convective breaking of internal waves. The role of a weak or strong stratification in the top part of the water column in convective breaking has been less investigated. This represents a motivation of the present study, where the wave-induced velocity field is evaluated for various density profiles with a pronounced variation close to the ocean surface. Conditions are identified where convective breaking is expected. More precisely, we determine when the computed horizontal fluid velocity becomes equal to the wave speed in terms of the wave amplitude and stratification.

The motion within the pycnocline is another important issue. Realistic predictions of the wave-induced velocity shear represent a first step in calculations of the dissipation and the associated mixing within the pycnocline. A model of these processes and the resulting thickening of the pycnocline was proposed by Bogucki & Garrett (1993). They assumed that shear instability would occur when the Richardson number dropped below 1/4, leading to breaking and mixing of the flow. The wave kinematics in their model was based on the Korteweg–de Vries equation and the Benjamin–Ono equation, and the pycnocline was assumed to be thin.

Instability of a steady stratified shear flow is found to be initiated when the Richardson number locally attains a value that is less than 1/4. Sometimes values less than 0.2 are needed. Experimental (Scotti & Corcos 1972) and numerical (Hazel 1972; Winters & D'Asaro 1989) confirmation has been given. Other instability mechanisms, like the Holmboe instability (Holmboe 1962; Browand & Wang 1972), may occur in stratified wave motion for any (large) value of the Richardson number if the shear layer is thick and the pycnocline thin. Parametric instability of time-periodic shear flow in a stably stratified fluid has been found for arbitrarily large Richardson numbers (Majda & Shefter 1998). Parametric resonance of periodic waves propagating along a density gradient has been the subject of several works (Davies & Acrivos 1967; McEvan & Robinson 1975; Mied 1976; Drazin 1977; Klostermeyer 1982).

We shall here study how the Richardson number Ri varies with the wave amplitude and the thickness of the pycnocline. This was recently studied by Stastna & Lamb (2002) including the effect of a background current. They represented the background density field by a tanh-profile and computed the value of the Richardson number in large waves as a function of the vertical coordinate. Our predictions indicate that the pycnocline thickness increases under large waves when the top layer is homogeneous, but decreases if the top layer is stratified. Another result is that the pycnocline thickness has relatively little influence on the minimum value of the Richardson number when this is close to 1/4. We shall identify the curve of minimal $Ri = 1/4$ as a function of the wave amplitude and stratification. Comparison with a limited set of laboratory experiments of solitary waves indicates that shear-induced breaking occurs for Ri somewhat less than 1/4. The present theoretical results may serve as guidance for a calibration of laboratory experiments on shear instability of solitary waves.

After our paper was submitted, Voronovich (2003) published a somewhat related model where two layers, each with constant buoyancy frequency, are separated by an interface, allowing for a jump in the tangential velocity across the interface. His set of equations is closed by enforcing a continuous pressure at the interface. Assuming long waves and weak stratifications, he made comparisons with fully nonlinear interface

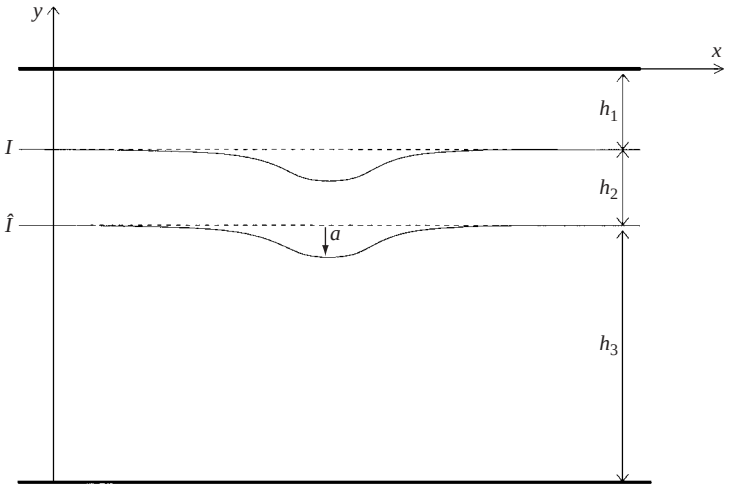

FIGURE 1. Sketch of the three-layer fluid. The wave amplitude a is defined as the maximum excursion of the interface $\hat{I}$ (and is a positive quantity).

models with homogeneous density layers and with observations from the COPE experiment (Stanton & Ostrovsky 1998). It has been documented previously that fully nonlinear interface computations with constant density in each layer provide an excellent explanation of the data from the COPE experiment, see Grue & Ostrovsky (2002), Ostrovsky & Grue (2003).

We derive a fully nonlinear mathematical procedure valid for a layered fluid where each layer has a constant buoyancy frequency. Computations are performed for two- and three-layer cases. The method represents an alternative to existing methods assuming a continuous buoyancy frequency (see e.g. Turkington *et al.* 1991, pp. 106, 117) and is motivated by conditions in nature where the buoyancy frequency is (almost) constant in an upper layer of the ocean, see e.g. Grue *et al.* (2000, figure 1). An additional motivation comes from laboratory studies of internal waves. Calibration of a layered fluid with uniform stratification in the layers is relatively controllable and works well for repetitions of the experiment.

We investigate in detail the case where the undisturbed stratification has one value of the Brunt–Väisälä frequency in the top part of the fluid, N_1, another Brunt–Väisälä frequency in the second layer, N_2, and a homogeneous fluid below, see figure 1 for illustration. The case $N_1 = N_2$, i.e. a two-layer fluid with a linear stratification in the upper layer and a homogeneous fluid in the lower was investigated theoretically and experimentally by Grue *et al.* (2000). Both theory and experiments showed that the wave-induced fluid velocity at the upper surface became equal to the wave velocity when the wave amplitude was 0.855 times the thickness of the upper stratified layer. The computations show that u/c could exceed unity, where u is the horizontal fluid velocity and c is the wave speed, while convective breaking occurred in the experiments when the experimental u/c was close to one. The experimental u was always limited by the wave speed c. A broadening of the (experimental) waves was observed when the limit $u/c = 1$ was reached. The theoretical results of this work are generalized here.

The motion within the pycnocline is studied in the case when the undisturbed fluid has a constant Brunt–Väisälä frequency in the mid-layer. Above is a homogeneous

or stratified layer which is limited above by a rigid lid. Computations are performed with both thin and broad pycnoclines.

The two-dimensional velocity field is determined from a stream function. This satisfies the Helmholtz equation in the layers with non-zero Brunt–Väisälä frequency and the Laplace equation if the layer is homogeneous. The stream function is expressed in terms of singularity distributions along the streamlines separating the layers. This results in a set of integral equations. The linear part of the integral equation operator is singular. The singular set of equations is inverted using Fourier transform. The conditioning of the system of equations is invoked by analytical means. It is found that a combination of Bessel functions of order zero, of the second and first kind, generally are required in the Green function in order to obtain a complete solution of the Helmholtz equation. The nonlinear, regular part of the equations is evaluated in the physical space for subsequent transform.

Following the Introduction, § 2 describes the mathematical model and § 3 the solution procedure using integral equations. In § 4 the fully nonlinear model is discussed with respect to weakly nonlinear theories. Section 5 presents computations of the flow in the pycnocline and in the top part of the water column with emphasis on potential breaking. Section 6 is a Conclusion.

2. Fully nonlinear theory

A three-layer model of a stably stratified fluid with a linear density profile in each layer is developed, coded and tested. The mathematical model is generalized to the case of a continuous density profile with an arbitrary (finite) number of layers, each with a constant Brunt–Väisälä frequency.

The layers in the three-layer model are referred to by numbers 1, 2 and 3 as indicated in figure 1. The indexes will be used for the physical parameters in the individual layers. We introduce a coordinate system O-xy with the horizontal x-axis on the top level of the fluid and the y-axis pointing upward. There are two interfaces: one separating layers 1 and 2, and one separating layers 2 and 3. The former we denote by I, and the latter by $\hat{I}$. A wave amplitude a is defined by the maximal excursion of the interface $\hat{I}$, and is a positive quantity. The layer thicknesses are h_1, h_2, h_3. The bottom of layer 3 is located at $y = -h_1 - h_2 - h_3$. The density profile at rest is determined by

$$\rho(y) = \begin{cases} \rho_0 - \Delta\rho_1 \dfrac{y + h_1}{h_1} - \Delta\rho_2, & -h_1 < y < 0, \\ \rho_0 - \Delta\rho_2 \dfrac{y + h_1 + h_2}{h_2}, & -h_1 - h_2 < y < -h_1, \\ \rho_0 - \Delta\rho_3 \dfrac{y + h_1 + h_2}{h_3}, & -h_1 - h_2 - h_3 < y < -h_1 - h_2, \end{cases} \tag{2.1}$$

where ρ_0 denotes the reference density of the fluid and $\Delta\rho_j$ perturbation densities. The Brunt–Väisälä frequency within each of the layers is determined by $N_j^2 = (\Delta\rho_j g)/(\rho_0 h_j)$, $j = 1, 2, 3$ (assuming $\Delta\rho_j/\rho_0 \ll 1$, see below). As a reference case, denoted by case (a), we let the density profile be determined by $N_1 = N_2$ and $N_3 = 0$. A second profile (b) is the most general, where the Brunt–Väisälä frequency is different in each of the layers. Finally, in a case (c), the upper and lower layers have zero Brunt–Väisälä frequency, i.e. $N_1 = 0$, $N_3 = 0$, while N_2 in the second layer is non-zero. The three different density profiles are visualized in figure 2.

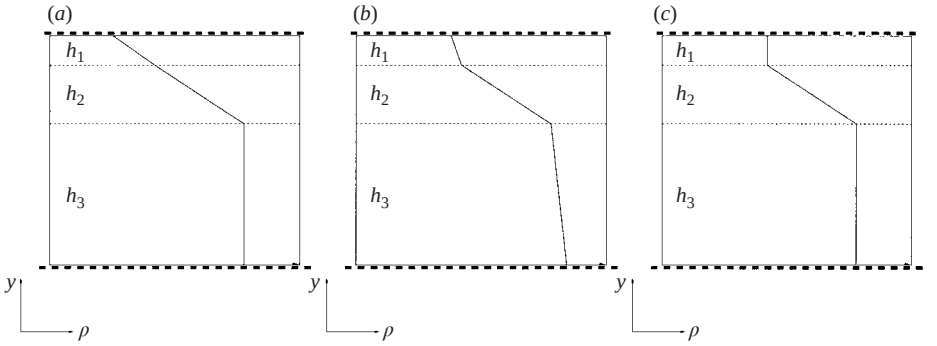

FIGURE 2. Models (*a*), (*b*) and (*c*).

Solitary waves of permanent form propagating horizontally with speed c in the fluid are considered. Viewing the problem in a frame of reference which follows the wave, the motion becomes steady. We assume, without loss of generality, that the flow in the far field is a current with speed c directed along the negative x-axis. We assume that the fluid is incompressible and inviscid. The former means that $\nabla \cdot \boldsymbol{v} = 0$ where $\boldsymbol{v} = (U, v)$ denotes the fluid velocity. Conservation of mass, $\nabla \cdot (\rho \boldsymbol{v}) = 0$, means that $\boldsymbol{v} \cdot \nabla \rho = 0$. A stream function representation of the velocity field is adopted, i.e. $U = \partial \Psi / \partial y = -c + \partial \psi / \partial y = -c + u$ and $v = -\partial \Psi / \partial x = -\partial \psi / \partial x$ where Ψ denotes the stream function and ψ the perturbation stream function. A streamline is a density contour since $\rho = \rho(\Psi)$ (and $\nabla \rho \cdot \nabla \Psi = 0$). The equation governing the perturbation stream function results from integrating the equation of motion of the fluid (Dubreil-Jacotin 1932; Long 1958; Yih 1960; Grue *et al.* 2000). We shall assume here that $\Delta \rho_j / \rho_0 \ll 1$, $j = 1, 2, 3$, such that the Boussinesq approximation can be made, which is relevant to oceanic conditions. In this case the motion in the body of the fluid is governed by

$$\nabla^2 \psi + \frac{N^2}{c^2} \psi = 0, \tag{2.2}$$

where N^2 is determined in each layer. The stream function ψ is conveniently represented by the stream functions ψ_1, ψ_2, ψ_3, where the indexes refer to layers 1, 2, 3.

The upper boundary of the top layer is approximated by a horizontal rigid lid. The internal-wave-induced deflection of a free surface may subsequently be estimated, see § 5.7. (When the aim is to model internal waves in the ocean, the top boundary of the mathematical model replaces a free surface. Since the internal wave speed, with $\Delta \rho / \rho_0 \ll 1$, is an order of magnitude less than the wave speed of free-surface waves of comparable wavelength, this supports the application of the rigid lid approximation there. This is also supported by experimental laboratory studies where there is no fundamental difference between internal solitary waves propagating along a pycnocline with the top of the fluid being either a free surface or covered by polystyrene. A surface tension is known to have an effect on wave breaking when the horizontal fluid velocity becomes close to the wave phase velocity, see Grue *et al.* (2000). The effect of a surface tension is not included in the mathematical model.) The rigid lid condition also applies at the bottom of the lower layer at $y = -h_1 - h_2 - h_3$, i.e.

$$\psi_1 = 0 \quad \text{at} \quad y = 0, \tag{2.3}$$

$$\psi_3 = 0 \quad \text{at} \quad y = -h_1 - h_2 - h_3. \tag{2.4}$$

Layers 1 and 2 are separated by the streamline with vertical coordinate $\eta - h_1$, where η denotes the vertical excursion of I from rest, and $\eta \to 0$ for $x \to \pm\infty$. Similarly, layers 2 and 3 are separated by the streamline with vertical coordinate $\hat{\eta} - h_1 - h_2$, where $\hat{\eta}$ denotes the vertical excursion of $\hat{I}$ from rest, and $\hat{\eta} \to 0$ for $x \to \pm\infty$.

The kinematic boundary condition requires that the normal velocity is continuous, and equal to zero, at the stationary boundaries between the layers. Since the total head, $H = p + \rho g y + \rho \frac{1}{2} \boldsymbol{v}^2$, is constant along each streamline, and since there is no jump in the density across the boundary between the layers, we may choose the tangential velocity to also be continuous there. Thereby the pressure is continuous at the boundaries I and $\hat{I}$, giving

$$\nabla(\psi_1 - cy) = \nabla(\psi_2 - cy) \quad \text{at} \quad y = \eta - h_1, \tag{2.5}$$

$$\nabla(\psi_2 - cy) = \nabla(\psi_3 - cy) \quad \text{at} \quad y = \hat{\eta} - h_1 - h_2. \tag{2.6}$$

Thus

$$\frac{\partial \psi_2}{\partial s} - c\frac{\partial \eta}{\partial s} = 0 \quad \text{at} \quad y = \eta - h_1, \tag{2.7}$$

$$\frac{\partial \psi_1}{\partial s} - c\frac{\partial \eta}{\partial s} = 0 \quad \text{at} \quad y = \eta - h_1, \tag{2.8}$$

$$\frac{\partial \psi_1}{\partial n} = \frac{\partial \psi_2}{\partial n} \quad \text{at} \quad y = \eta - h_1 \tag{2.9}$$

$$\frac{\partial \psi_3}{\partial s} - c\frac{\partial \hat{\eta}}{\partial s} = 0 \quad \text{at} \quad y = \hat{\eta} - h_1 - h_2, \tag{2.10}$$

$$\frac{\partial \psi_2}{\partial s} - c\frac{\partial \hat{\eta}}{\partial s} = 0 \quad \text{at} \quad y = \hat{\eta} - h_1 - h_2, \tag{2.11}$$

$$\frac{\partial \psi_2}{\partial n} = \frac{\partial \psi_3}{\partial n} \quad \text{at} \quad y = \hat{\eta} - h_1 - h_2, \tag{2.12}$$

where s denotes the arc length along the streamlines I and $\hat{I}$ and n the normal, pointing out of layer 2 into layer 1, and pointing out of layer 3 into layer 2. The formulation is fully nonlinear, where the stream functions $\psi_{1,2,3}$ and the streamlines η, $\hat{\eta}$ are to be determined.

3. Solution by integral equations

We solve the nonlinear problem (2.2)–(2.12) by means of integral equations. Green functions G_1, G_2, G_3 in each of the layers are introduced. The relevant Green function in the upper layer has a pole at $(x, y) = (x', y')$, and satisfies the Helmholtz equation (2.2) and the rigid lid condition at $y = 0$, i.e.

$$G_1(x, y, x', y') = \frac{\pi}{2}[Z_0(\alpha_1, K_1 r) - Z_0(\alpha_1, K_1 r_1)], \tag{3.1}$$

where $K_1 = N_1/c$, $r = [(x - x')^2 + (y - y')]^{1/2}$ and $r_1 = [(x - x')^2 + (y + y')^2]^{1/2}$. The function Z_0 is defined by

$$Z_0(\alpha, \hat{x}) = Y_0(\hat{x}) + \alpha J_0(\hat{x}) \tag{3.2}$$

where J_0 and Y_0 denote the Bessel functions of order zero, of the first and second kind, respectively, and α a real constant to be chosen. The importance of the non-singular term $\alpha J_0(\hat{x})$ is discussed below. Z_0 behaves like $\ln(K_1 r)$ for $K_1 r \to 0$. In what follows

we shall also use the function $Z_1(\alpha, \hat{x}) = Y_1(\hat{x}) + \alpha J_1(\hat{x})$. In the cases with $N_1 = 0$ in the upper layer, the appropriate Green function is $G_1(x, y, x', y') = \ln(r/r_1)$.

In the second layer, the Green function is

$$G_2(x, y, x', y') = \frac{\pi}{2} Z_0(\alpha_2, K_2 r), \tag{3.3}$$

where $K_2 = N_2/c$. Finally, in layer three we have

$$G_3(x, y, x', y') = \frac{\pi}{2}(Z_0(\alpha_3, K_3 r) - Z_0(\alpha_3, K_3 r_3)), \tag{3.4}$$

where $K_3 = N_3/c$, $r_3 = [(x - x')^2 + (y + y' + 2H_3)^2]^{1/2}$ and $H_3 = h_1 + h_2 + h_3$. If $N_3 = 0$, $G_3(x, y, x', y') = \ln(r/r_3)$.

Let the stream functions ψ_1, ψ_2, ψ_3 be determined by singularity distributions:

$$\psi_1 = \int_I \sigma_1(s') G_1(x, y, x'(s'), y'(s'))\, \mathrm{d}s', \tag{3.5}$$

$$\psi_2 = \int_I \sigma_2(s') G_2(x, y, x'(s'), y'(s'))\, \mathrm{d}s' + \int_{\hat{I}} \hat{\sigma}_2(s') G_2(x, y, x'(s'), y'(s'))\, \mathrm{d}s', \tag{3.6}$$

$$\psi_3 = \int_{\hat{I}} \sigma_3(s') G_3(x, y, x'(s'), y'(s'))\, \mathrm{d}s', \tag{3.7}$$

where $\sigma_1(s)$, $\sigma_2(s)$ $\hat{\sigma}_2(s)$ and $\sigma_3(s)$ denote unknown distributions. The kinematic and dynamic boundary conditions (2.7)–(2.9) give, at I,

$$\barint_I \sigma_1(s') \frac{\partial G_1}{\partial s}\, \mathrm{d}s' - c\frac{\partial \eta}{\partial s} = 0, \tag{3.8}$$

$$\barint_I \sigma_2(s') \frac{\partial G_2}{\partial s}\, \mathrm{d}s' + \int_{\hat{I}} \hat{\sigma}_2(s') \frac{\partial G_2}{\partial s}\, \mathrm{d}s' - c\frac{\partial \eta}{\partial s} = 0, \tag{3.9}$$

$$\pi[\sigma_1(s) + \sigma_2(s)] + \int_I \left(\sigma_1(s') \frac{\partial G_1}{\partial n} - \sigma_2(s') \frac{\partial G_2}{\partial n}\right) \mathrm{d}s' - \barint_{\hat{I}} \left(\hat{\sigma}_2(s') \frac{\partial G_2}{\partial n}\right) \mathrm{d}s' = 0, \tag{3.10}$$

where a bar on the integral sign denotes principal value. Correspondingly, the kinematic boundary conditions (2.10)–(2.12) give at $\hat{I}$

$$\int_I \sigma_2(s') \frac{\partial G_2}{\partial s}\, \mathrm{d}s' + \barint_{\hat{I}} \hat{\sigma}_2(s') \frac{\partial G_2}{\partial s}\, \mathrm{d}s' - c\frac{\partial \hat{\eta}}{\partial s} = 0, \tag{3.11}$$

$$\barint_{\hat{I}} \sigma_3(s') \frac{\partial G_3}{\partial s}\, \mathrm{d}s' - c\frac{\partial \hat{\eta}}{\partial s} = 0, \tag{3.12}$$

$$\pi[\hat{\sigma}_2(s) + \sigma_3(s)] + \int_{\hat{I}} \left(\hat{\sigma}_2(s') \frac{\partial G_2}{\partial n} - \sigma_3(s') \frac{\partial G_3}{\partial n}\right) \mathrm{d}s' + \barint_I \left(\sigma_2(s') \frac{\partial G_2}{\partial n}\right) \mathrm{d}s' = 0. \tag{3.13}$$

A pseudo-spectral method based on a Fourier transform is employed to solve the mathematical problem. The functions are represented in terms of the horizontal x-coordinate. The waves are considered here to be non-overhanging, a restriction that may be removed by using the arc lengths of I and $\hat{I}$ as variables. The Fourier transformed equations and the computational procedure are described in an Appendix.

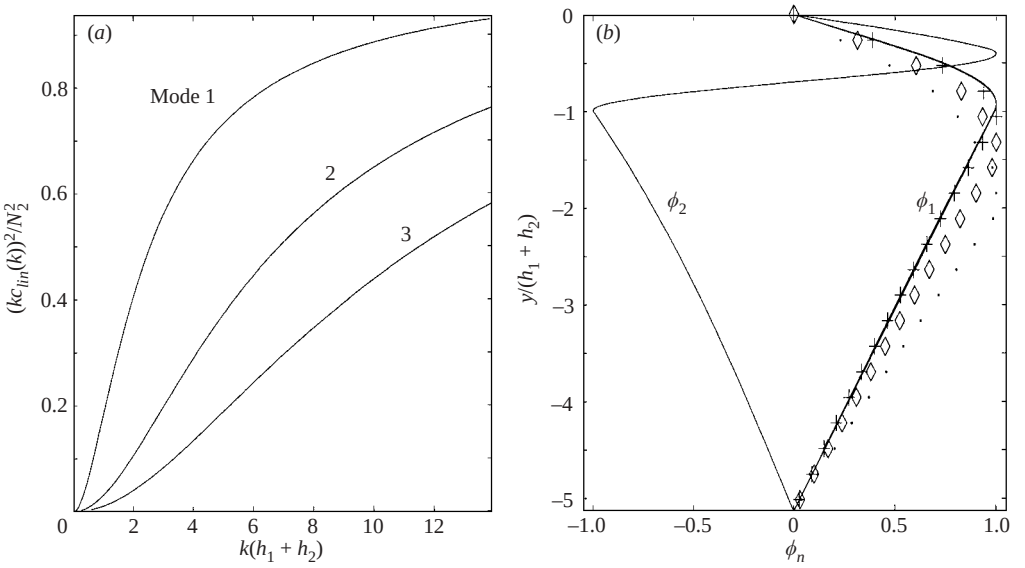

FIGURE 3. (*a*) Dispersion curves for the first three modes. (*b*) Long-wave normalized eigenfunctions and fully nonlinear normalized 'mean stream function' for $a/(h_1+h_2)=0.05$ (+), 0.5 ($\diamond$), 1 ($\cdots$). Stratification case (*b*) with $N_1/N_2=0.5$, $N_3=0$. $h_3/(h_1+h_2)=4.13$ and $h_2/h_1=2$.

4. Linear and weakly nonlinear theory

4.1. *Linear theory*

Linear theory is a reference when the wave amplitude is very small. Assuming for the moment that the wave train is periodic with wavenumber k and (linear) wave speed c_{lin}, the stream function is of the form $\psi(x,y)=a_0\phi(y)\exp(\mathrm{i}kx)$ where a_0 denotes amplitude. The function ϕ is determined by the eigenvalue problem

$$\left[\frac{\mathrm{d}^2}{\mathrm{d}y^2}+\frac{N^2}{c_{lin}^2}-k^2\right]\phi=0, \tag{4.1}$$

where in addition the following boundary conditions apply: $\phi(0)=\phi(-h_1-h_2-h_3)=0$. The functions ϕ and $\mathrm{d}\phi/\mathrm{d}y$ are continuous at the two interfaces. Solution of the Taylor–Goldstein equation (4.1) takes the form $A_j\cos(\hat{K}_j y)+B_j\sin(\hat{K}_j y)$ in each layer, where $\hat{K}_j=\sqrt{N_j^2/c_{lin}^2-k^2}$, $j=1,2,3$, and A_j and B_j are constants. The dispersion relation $c_{lin}(k)$ is obtained by using the boundary conditions at $y=0$, $y=-h_1$, $y=-h_1-h_2$, $y=-h_1-h_2-h_3$, giving

$$\hat{K}_2^2-T_1T_2-T_1T_3-T_2T_3=0, \qquad T_j=\hat{K}_j\cot(\hat{K}_j h_j). \tag{4.2}$$

Linear dispersion curves and eigenfunctions are shown in figure 3, which includes computations of the nonlinear first mode eigenfunction in the long-wave limit ($k=0$). This is obtained from the Fourier transform of the fully nonlinear numerical solution, for zero wavenumber, i.e. by $\int_{-\infty}^{\infty}\psi(x,y)\,\mathrm{d}x$. Figure 3(*b*) shows that the peak of nonlinear eigenfunction is moved downwards in the fluid, in accordance with the wave-induced excursion of the streamlines.

4.2. *The linear long-wave speed*

The linear long-wave speed, c_0, is a reference for the nonlinear computations and is obtained from (4.2) by letting $k \to 0$. In the special case (a), where $N_1 = N_2$ and $N_3 = 0$, the linear long-wave speed is determined by $\cot(X) + (h_1 + h_2)/(h_3 X) = 0$ where $X = \hat{K}_1(h_1 + h_2)$ (and $k = 0$). The fastest wave mode is determined for X in the interval $(\pi/2, \pi)$ (Grue *et al.* 2000). In case (c), with $N_1 = N_3 = 0$, (4.2) simplifies to $\cot(Y) - [Yh_1/h_2 - h_2/(h_3 Y)]/[1 + h_1/h_3] = 0$ where $Y = \hat{K}_2 h_2$ (and $k = 0$). The longest wave mode is obtained for Y in the interval $(0, \pi)$.

4.3. *Weakly nonlinear models*

The fully nonlinear computations may be put in the framework of weakly nonlinear theory, e.g. the Korteweg–de Vries (KdV) equation. In a fixed frame of reference this is (see e.g. Pelinovsky, Poloukhina & Lamb 2000)

$$\frac{\partial a_0}{\partial t} + c_0 \frac{\partial a_0}{\partial x} + \alpha_0 a_0 \frac{\partial a_0}{\partial x} + \beta \frac{\partial^3 a_0}{\partial x^3} = 0, \tag{4.3}$$

where $a_0(x, t)$ denotes the amplitude function. This is related to the stream function by $\psi(x, y, t) = a_0(x, t)\phi(y)$ where $\phi(y)$ is the solution of the eigenvalue problem (4.1) (with $k = 0$). The coefficients in (4.3) are, in the Boussinesq approximation, obtained from

$$\alpha_0 = \frac{3}{2} c_0 \int_{-H}^{0} \phi_y^3 \, \mathrm{d}y \Big/ \int_{-H}^{0} \phi_y^2 \, \mathrm{d}y, \quad \beta = \frac{1}{2} c_0 \int_{-H}^{0} \phi^2 \, \mathrm{d}y \Big/ \int_{-H}^{0} \phi_y^2 \, \mathrm{d}y$$

where the notation $\phi_y = \mathrm{d}\phi/\mathrm{d}y$, $H = h_1 + h_2 + h_3$ is used. The solitary wave solution of (4.3) propagating with speed c is well known: $a_0(x - ct) = -\hat{a}_0 \operatorname{sech}^2((x - ct)/\lambda)$, where $c = c_0 + \hat{a}_0\alpha_0/3$ and $\lambda^2 = 12\beta/(\alpha_0 \hat{a}_0)$.

Weakly and fully nonlinear computations of the wave speed and the (horizontal) velocity profile at a crest are compared in figure 4. The fluid is characterized by $N_1 = N_3 = 0$ and $h_3/(h_1 + h_2) = 4.13$, $h_2/h_1 = 2$. There is good agreement between KdV theory and the fully nonlinear solution when the solitary wave amplitude is small ($a/(h_1 + h_2) = 0.05$). A significant deviation in the velocity profile is observed for $a/(h_1 + h_2) = 0.5$, however. It is evident that the main problem with the weakly nonlinear theory is the lack of account taken of a finite excursion of the streamlines, induced by the wave motion, see also the discussion by Ostrovsky & Grue (2003).

We briefly compare weakly and fully nonlinear results for the wave width $w_{1/2}$ of solitary waves. The wave width is the average width of the two isolines I and $\hat{I}$, where the width of each is defined to be twice the distance from the centre of the wave at which the vertical displacement is half the maximum value. Fully nonlinear computations are presented in figure 5(a), for stratified fluid with $N_1 = N_3 = 0$, $N_2 \neq 0$, $0 < h_2/h_1 < 1.83$. An increasing thickness of the pycnocline somewhat reduces the non-dimensional wave width $w_{1/2}/(h_1 + \frac{1}{2}h_2)$. This is true for moderate and large wave amplitudes. For waves of small amplitude there is no such effect, however. The present computations are also compared with results obtained using the two-layer interface model by Grue *et al.* (1999). There is excellent agreement when $h_2/h_1 \to 0$.

The fully nonlinear computations are also compared with weakly nonlinear KdV theory and Benjamin–Ono theory. The results in figures 5(b) and 5(c) are obtained for two-layer fluid with $N_1 = N_3 = 0$, $N_2 = \infty$, $h_2 = 0$ and $h_3/h_1 = 20.4$, 500, using the two-layer interface model by Grue *et al.* (1999). The weakly nonlinear theories work well only for waves of very small amplitude. Further comparisons with strongly nonlinear extensions of KdV theory are discussed in Ostrovsky & Grue (2003).

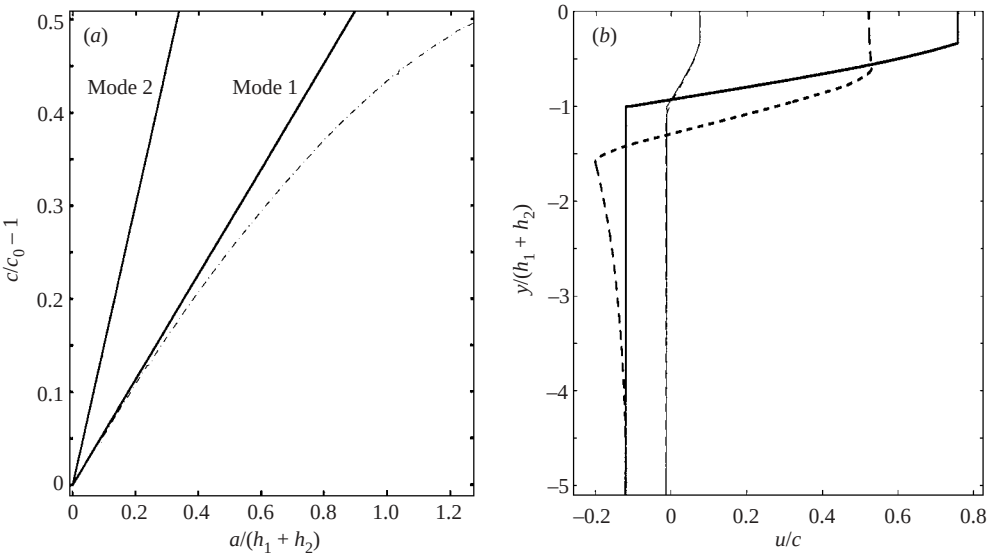

FIGURE 4. (*a*) Excess speed function of the amplitude compared with K-dV solutions for the two first modes. (*b*) Horizontal velocity at the crest for fully nonlinear computations (dashed lines) compared with result from K-dV for the first mode and amplitude $a/(h_1+h_2)=0.05$ (thin lines) and $a/(h_1+h_2)=0.5$ (thick lines). Stratification case (*c*), $h_3/(h_1+h_2)=4.13$ and $h_2/h_1=2$.

5. Discussion of fully nonlinear results

5.1. *Effect of a thin layer on top of a pycnocline*

We investigate first the effect of a thin homogeneous layer on top of a pycnocline of finite thickness. Computations are performed for a density profile of case (*c*) with $N_1=N_3=0$ and $N_2\neq 0$, see figure 2. Complementary computations with the density profile of case (*b*), with the ratio N_1/N_2 gradually varying from zero to unity, and with N_3 put to zero in the lower layer, are performed. The computations with $N_1/N_2=1$ and $N_3=0$ should agree with computations for the density profile of case (*a*), providing a check of the results. A depth ratio of $h_3/(h_1+h_2)=4.13$ is chosen, enabling a close comparison with the theoretical and experimental results given by Grue *et al.* (2000). Other depth ratios are also investigated.

The streamlines and vorticity field for a large-amplitude wave with $N_1=N_3=0$, $N_2\neq 0$ are shown in figure 6. The velocity gradient is pronounced within the pycnocline but is small in the upper and lower layers.

Velocity profiles at the wave crest with N_1/N_2 gradually increasing from zero to unity are shown in figure 7. A pronounced velocity gradient is observed only for a non-zero local Brunt–Väisälä frequency (just below the pycnocline a moderate velocity gradient is always present). A jump of the Brunt–Väisälä frequency induces a jump in the velocity gradient. The wave-induced fluid velocity may exceed the wave speed with $N_1/N_2=1$, thus inducing a convective breaking of the flow (Grue *et al.* 2000). A corresponding result is not found with a top layer with $N_1=0$. All computations performed with the three-layer model with $N_1=N_3=0$ and $N_2\neq 0$ exhibit a horizontal velocity that never exceeds c. This is also true if N_1/N_2 is small (see figure 7*c*). The latter result may be obtained analytically by invoking conservation

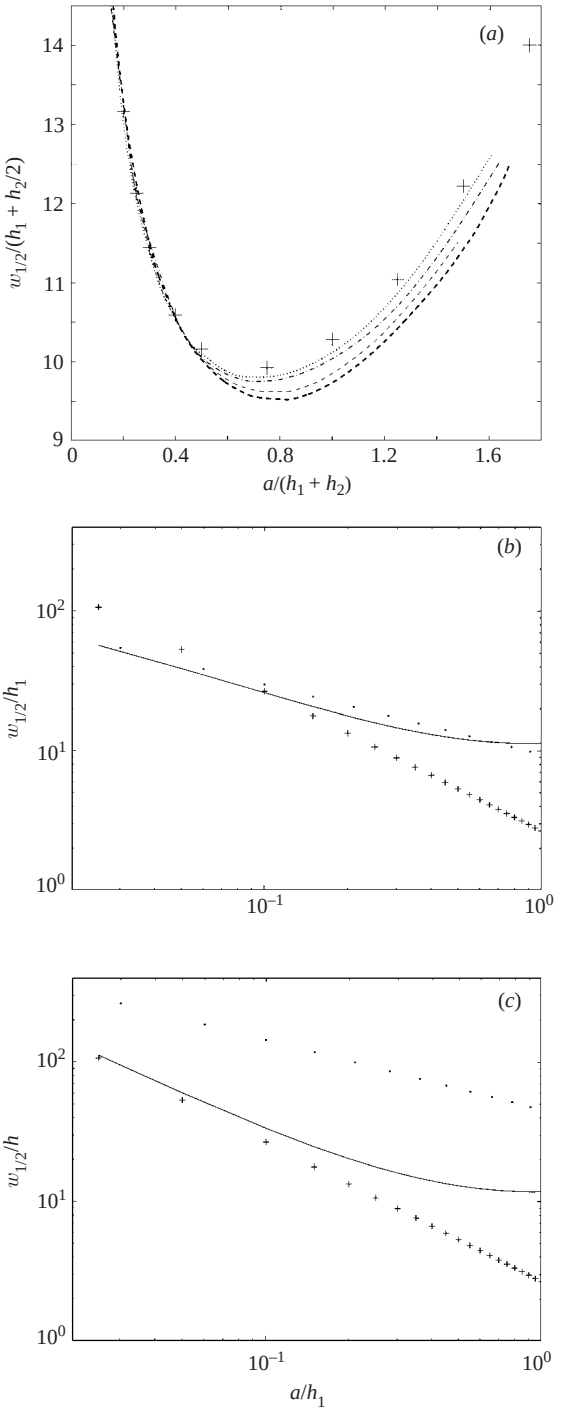

FIGURE 5. (*a*) Wave width vs. amplitude computed for several ratios h_2/h_1 for $(h_3+h_2/2)/(h_1+h_2/2)=5.7$ and $h_2/h_1=1.83$ (thick dashed line), 1.28 (dashed), 0.87 (dash-dotted), 0.56 (dotted) and compared with fully nonlinear two-layer model (Grue *et al.* 1999) $h_2/h_1=0$ (crosses). $N_1=N_3=0$, $N_2\neq 0$. (*b*) Wave width vs. amplitude. $h_3/h_1=20.4$ and $h_2=0$. $N_1=N_3=0$, $N_2\neq 0$. Results from K-dV (dots), Benjamin–Ono (crosses) compared with the fully nonlinear two-layer method by Grue *et al.* (1999). (*c*) Same as (*b*) but $h_3/h_1=500$.

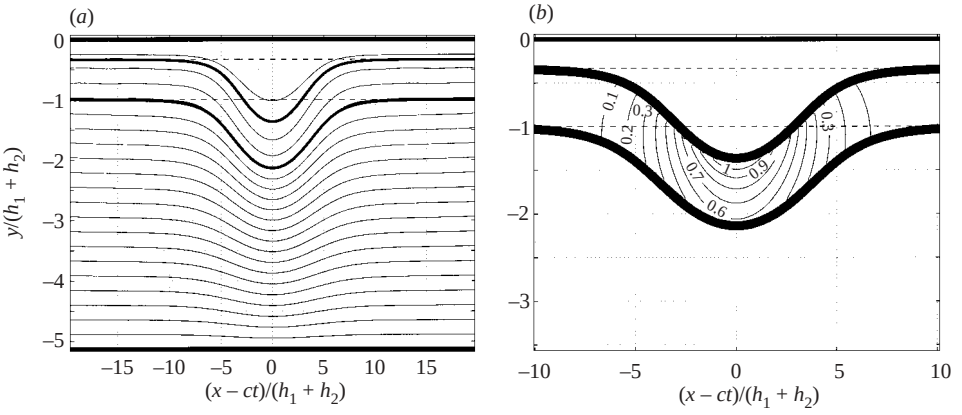

FIGURE 6. Case (c), streamlines (a) and vorticity $\omega/(2\hat{N})$ (b) in the domain. $h_2/h_1=2$, $h_3/(h_1+h_2)=4.13$, $a/(h_1+h_2)=1.15$. $\hat{N}$ is defined (5.1).

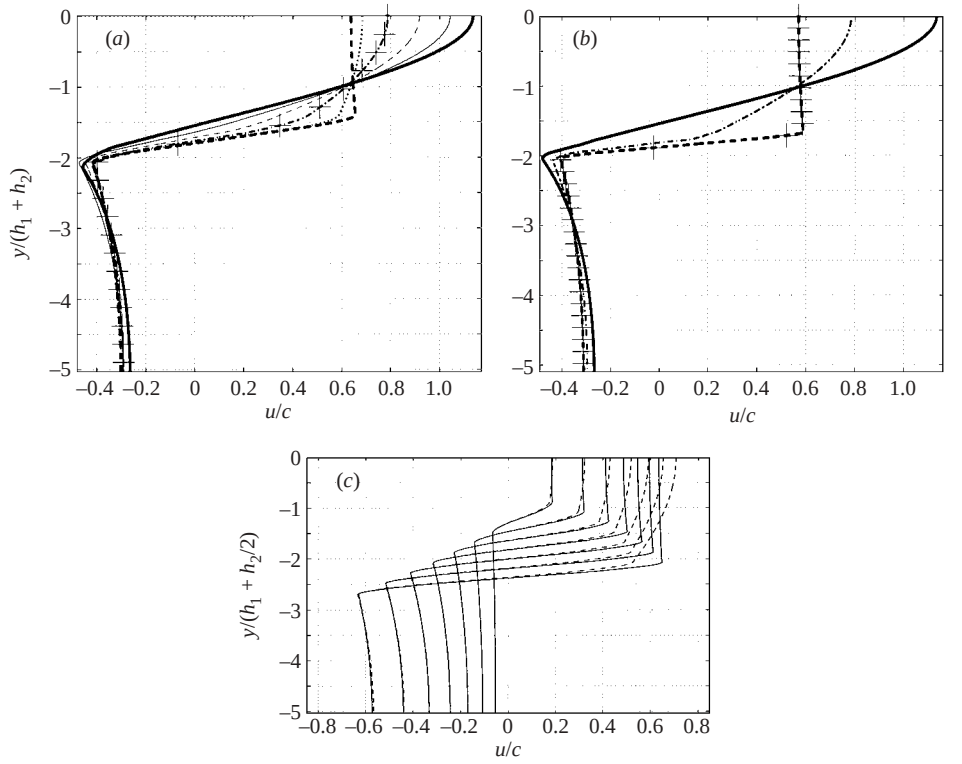

FIGURE 7. (a) Velocity profile at the crest for several values of N_1/N_2, $h_3/(h_1+h_2)=4.13$ and $a/(h_1+h_2)=1$. $h_2/h_1=0.87$: $N_1/N_2=1$ (thick solid line), 0.87 (solid), 0.7 (dashed), 0.5 (dash-dotted), 0.3 (dotted) and $N_1/N_2=0$ (thick dashed). (b) As (a) but $h_2/h_1=0.36$: $N_1/N_2=1$ (thick solid line), 0.5 (dash-dotted) and $N_1/N_2=0$ (thick dashed line). Computations are performed with 128 and 256 collocation points (a and b), respectively) while the crosses correspond to similar computations with 256 and 512 collocations points, respectively. (c) Velocity profile at the crest for amplitudes $a/(h_1+h_2/2)=0.2, 0.4, \ldots, 1.4$ and $h_2/h_1=0.5$, $(h_3+h_2/2)/(h_1+h_2/2)=4.13$. Solid lines: simulations with $N_3=0$ and $N_1/N_2=0.3$. Dashed lines: simulations with $N_1=N_3=0$, $N_2\neq 0$.

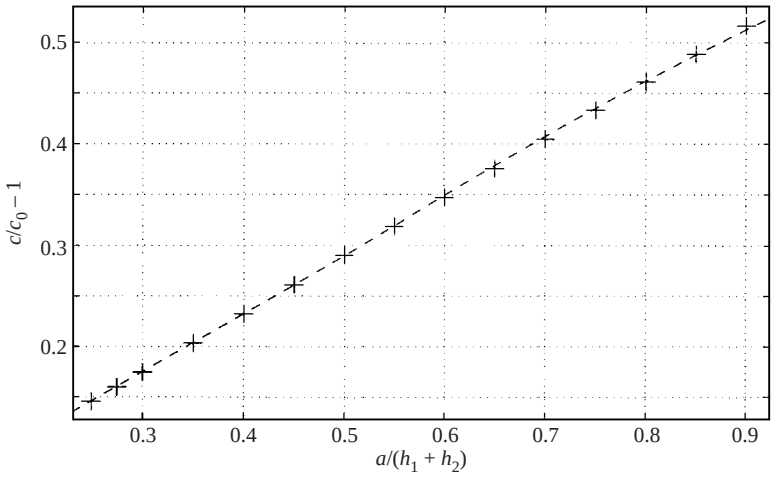

FIGURE 8. Propagation speed vs. wave amplitude. $h_3/(h_1+h_2)=4.13$, $N_1/N_2=1$, $N_3=0$. Comparison between present numerical scheme (dashed line), and the numerical scheme described in Grue *et al.* (2000) (crosses).

of mass in the top layer, assuming a horizontal velocity that is almost uniform in the vertical direction (when $N_1=0$).

In figure 7 we also compare velocity profiles obtained by the three different methods for the stratifications of cases (*a*), (*b*) and (*c*), respectively. The results with the different methods are indistinguishable. Convergence is documented by comparing computations with 128, 256 and 512 collocation points. The present model predictions with $N_1/N_2=1$ agree with the two-layer results obtained by Grue *et al.* (2000) (figure 8).

5.2. *Wave speed and thickness of the pycnocline*

All the computations we have performed show that the wave speed increases with increasing ratio N_1/N_2 between the Brunt–Väisälä frequencies in the two upper layers (figures 9 and 10). The ratio N_1/N_2 is varied in the range [0, 1.4], keeping N_2 fixed.

Computations of the pycnocline thickness at the maximal excursion of the wave show that this always decreases with increasing ratio N_1/N_2. In the case when the Brunt–Väisälä frequency in the top layer is zero ($N_1=0$), the pycnocline slightly increases with amplitude. For large-amplitude waves and $N_1/N_2=1$ the middle layer always becomes thinner at the wave crest than in the far field (figure 9). This effect is weaker for a large depth ratio $h_3/(h_1+h_2)$ than for a small one (figure 10). A relatively high resolution is required to obtain convergent results (figure 11).

5.3. *Horizontal velocity and vorticity*

The wave-induced horizontal velocity u relative to the wave speed c is evaluated at the surface ($y=0$). This function shows a monotonic growth with amplitude. Computations with $N_1/N_2=1$ and $N_3=0$ show that u/c exceeds unity when $a/(h_1+h_2)$ exceeds 0.855 (figure 12). When $N_1=N_3=0$ and $N_2\neq 0$, u/c is always less than unity (figure 12).

Figure 12(*a*) shows computations of u/c for N_1/N_2 in the range 0–1.53. All computations show that u/c exceeds unity when $N_1/N_2>0.45$, for sufficiently large amplitude. Beyond the amplitude with $u/c=1$ convective breaking is expected to occur. Convective breaking induced by the motion of a solitary wave was

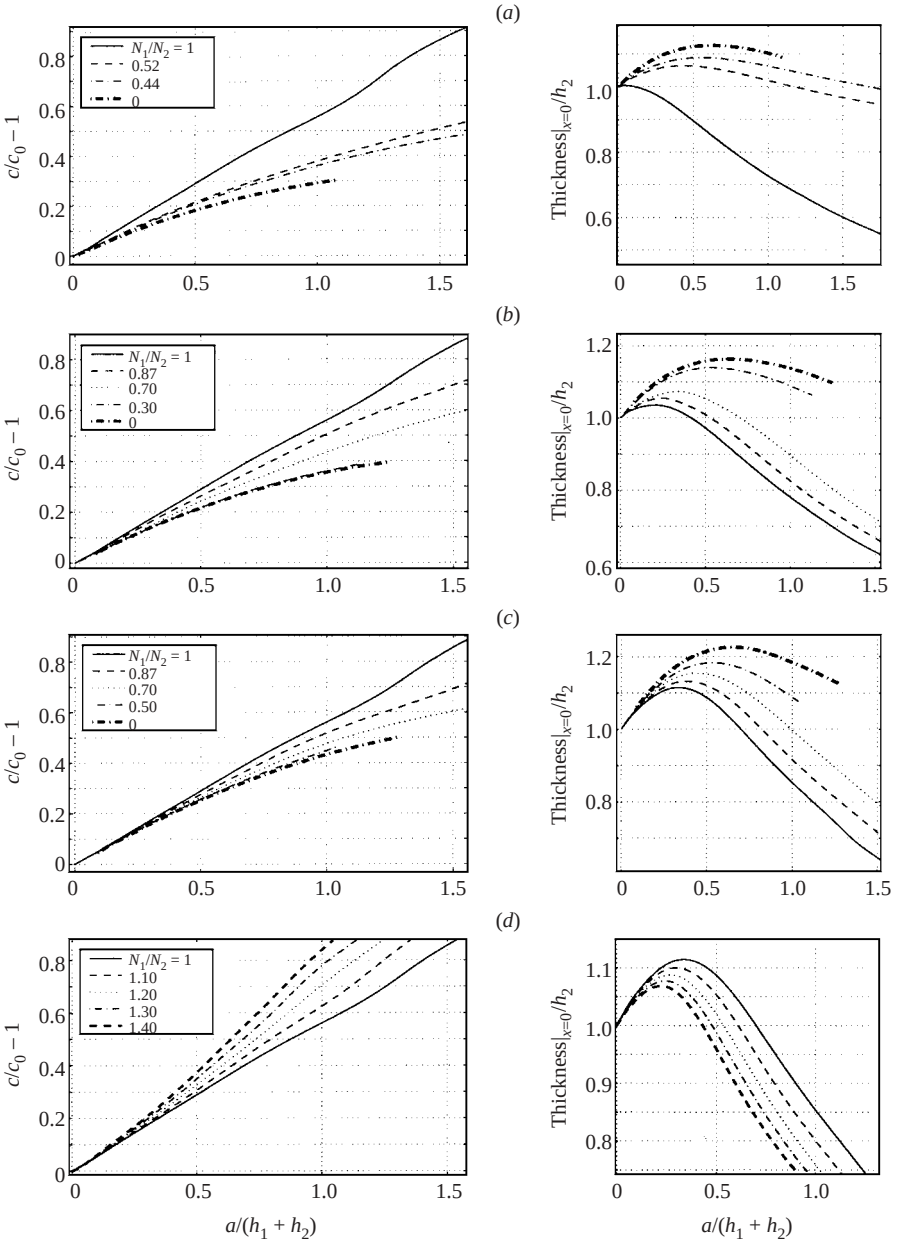

FIGURE 9. Excess speed and pycnocline thickness vs. amplitude. $0 \leqslant N_1/N_2 \leqslant 1$: (*a*) $h_2/h_1 = 0.36$, (*b*) $h_2/h_1 = 0.87$, (*c*) $h_2/h_1 = 2$. In (*d*) $1 \leqslant N_1/N_2 \leqslant 1.40$ and $h_2/h_1 = 2$. In all plots $h_3/(h_1 + h_2) = 4.13$.

experimentally documented by Grue *et al.* (2000) when the induced u became equal to c. In all our computations in which u/c exceeds 1, u/c first equals 1 at the surface. This indicates that an overturning of the waves will happen first in the upper part of the water column.

The wave-induced velocity shear represents a source of instability that may introduce a breaking of the flow. The velocity shear is quantified in terms of the

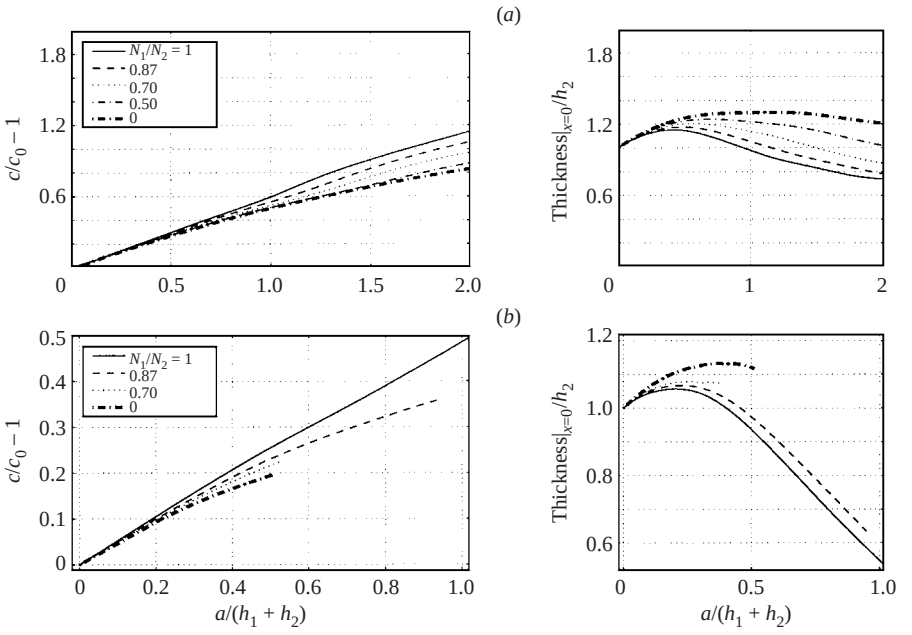

FIGURE 10. Excess speed and pycnocline thickness vs. amplitude for decreasing values of N_1/N_2. $h_3/(h_1+h_2) =$ 10 (*a*) and 2 (*b*); $h_2/h_1 = 2$.

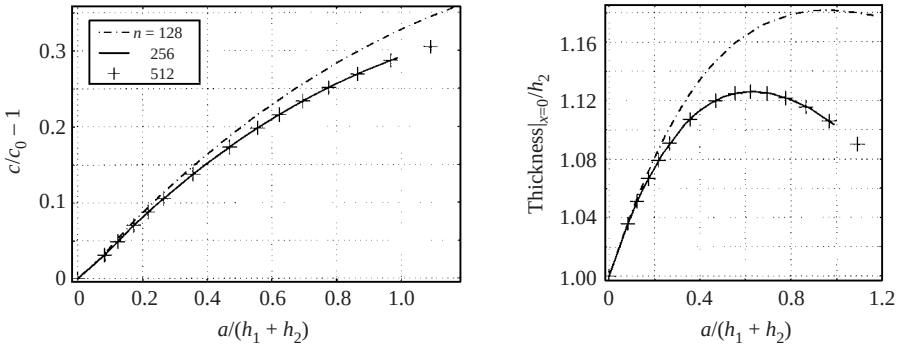

FIGURE 11. Excess speed and pycnocline thickness vs. amplitude for different resolutions. Number of collocation points: $n = 128$ (dash-dotted line), 256 (solid) and 512 (crosses). $N_1/N_2 = 0$; $h_2/h_1 = 0.36$; $h_3/(h_1+h_2) = 4.13$.

local vorticity ω which is evaluated using (2.2). A reference is the local Brunt–Väisälä frequency, $\hat{N}$, which is obtained using the fact that $\mathrm{d}\rho/\mathrm{d}\Psi$ is constant along a streamline, giving $\partial\rho/\partial y = (\mathrm{d}\rho/\mathrm{d}\Psi)_\infty(-c+u)$. This means that the local Brunt–Väisälä frequency is given by

$$\hat{N} = N_j\sqrt{1-u_j/c}, \qquad j = 1, 2, 3, \tag{5.1}$$

where N_j denotes the constant Brunt–Väisälä frequency in the far field. The value of the local Richardson number $Ri = \hat{N}^2/\omega^2$ indicates the ratio between the stabilizing effect of a stratification and the destabilizing effect of an unstable velocity profile.

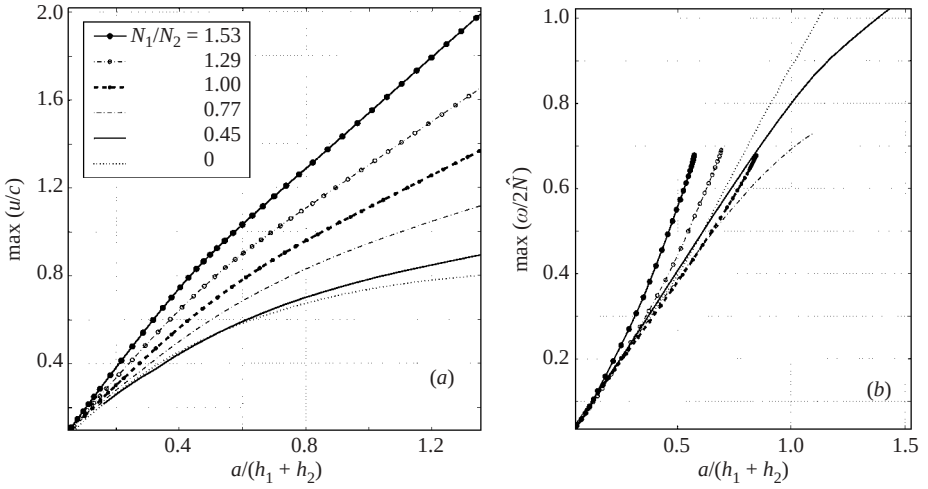

FIGURE 12. Maximum local velocity (a) and maximum local vorticity (b) vs. amplitude for $0 \leqslant N_1/N_2 \leqslant 1.53$, $N_3 = 0$. $h_2/h_1 = 2$, $h_3/(h_1 + h_2) = 4.13$.

Using (2.2), (5.1) and further that the stream function is related to the wave-induced vertical excursion δ of an isopycnal line by $\psi/c = \delta = y - y_\infty$, we have

$$Ri = \frac{c(c-u_j)}{N_j^2 \delta^2}, \qquad j = 1, 2, 3. \tag{5.2}$$

A main contribution to a small Ri is thus a large excursion δ of the isopycnal line. A minimal value of Ri occurs in the main body of the fluid. A small value of $c - u_j$ is less important since the corresponding value of δ is small, making Ri large. This is typically true close to the top and bottom of the fluid where $\delta \to 0$. (In the special case when $c - u_1 \to 0$ for $y \to 0$, we have that $c - u_1 \simeq \frac{1}{2}([\partial^2 u/\partial y^2]_{y=0})y^2$ and $\psi/c \simeq y = \delta$, giving $Ri < \infty$ when $y \to 0$).

A stationary parallel flow is stable when Ri is greater than $1/4$. Conversely, the flow may become unstable due to a shear instability if $Ri < 1/4$. It is of interest to identify when $Ri > 1/4$ for the slowly varying velocity field induced by the solitary wave. Values of $Ri > 1/4$ correspond to $\omega/2\hat{N} < 1$, since $\omega/2\hat{N} = \frac{1}{2} Ri^{-1/2}$.

Figure 12(b) shows computations of $\omega/2\hat{N} = \frac{1}{2} N_j |\delta| / \sqrt{c^2 - cu}$ for N_1/N_2 in the range 0–1.53. In all examples the quantity grows monotonically with amplitude. The maximal value of $\omega/2\hat{N}$ exceeds unity in the computations with $N_1/N_2 = 0$ and 0.45, when the wave amplitude is sufficiently large. For values of $N_1/N_2 \geqslant 0.77$, $\omega/2\hat{N}$ is always less than 1.

It is of interest to identify wave parameters when u/c and $\omega/2\hat{N}$ are both less than unity. The wave-induced flow is then expected to be stable (non-breaking). Conversely, for $u/c > 1$ or $\omega/2\hat{N} > 1$ the flow may exhibit breaking. The computations may be useful for calibration of e.g. breaking internal wave experiments. They may further be used to interpret observations of breaking internal solitary waves at large scale.

Figure 13(a) plots $\omega/2\hat{N} = 1$ (corresponding to $Ri = 1/4$) and $u/c = 1$ as function of non-dimensional wave amplitude $a/(h_1 + h_2)$ and N_1/N_2. The depth ratio $h_3/(h_1 + h_2)$ is 4.13 and h_2/h_1 is between 0.36 and 2. Results with different thicknesses of the pycnocline show that the wave-induced flow is expected to be stable when the non-dimensional wave amplitude $a/(h_1 + h_2)$ is up to about unity. A thick pycnocline is

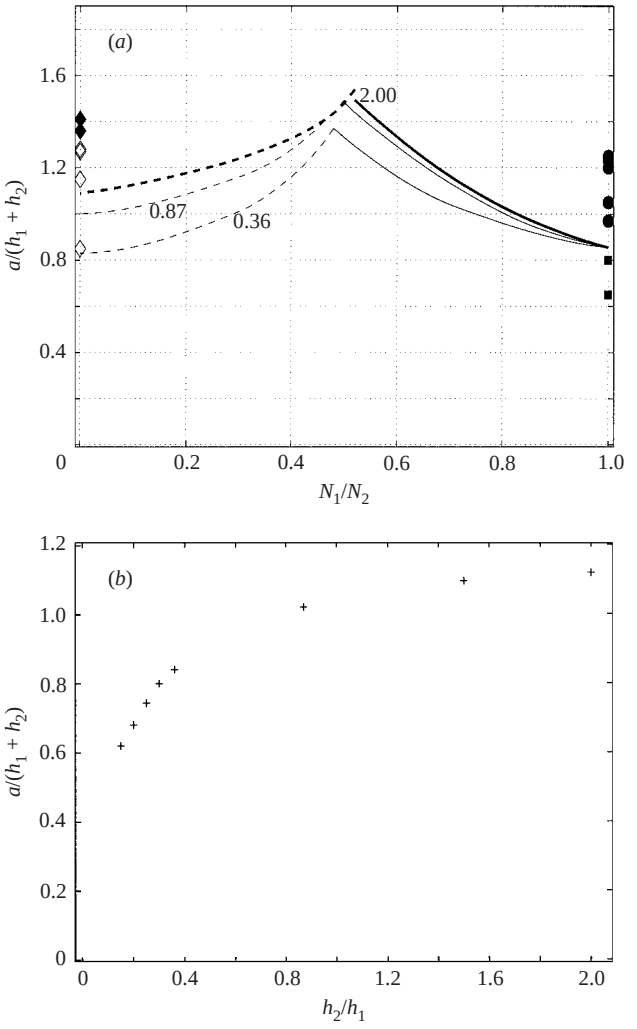

FIGURE 13. (*a*) Lines with $\omega/2\hat{N}=1$ (dashed) and $u_{1max}/c=1$ (solid) as function of $a/(h_1+h_2)$ and N_1/N_2, $N_3=0$. $h_2/h_1=0.36, 0.87, 2$. $h_3/(h_1+h_2)=4.13$. Observations of shear instability (filled diamonds) and no instability (open diamonds) from Grue *et al.* (1999). Observations of convective breaking from Grue *et al.* (2000) (filled circles). Convective breaking provoked by the effect of a surface tension (Grue *et al.* 2000) (filled squares). (*b*) Amplitude at which $\omega/2\hat{N}=1$ vs. h_2/h_1. $N_1=N_3=0$, $h_3/(h_1+h_2)=4.13$.

only slightly more stabilizing than a pycnocline that is moderately thin. A stratified top layer represents a weak stabilizing effect when N_1/N_2 is increasing up to about 0.5, but becomes destabilizing for N_1/N_2 larger than about 0.5. Figure 13(*b*) plots $\omega/2\hat{N}=1$ for $N_1=0$ and h_2/h_1 in the range from 0.15 to 2. A very thin pycnocline somewhat reduces the range of stability.

Supplementary computations of $\omega/2\hat{N}=1$ and $u/c=1$ for deep and shallow lower layers are shown in figure 14. The amplitude range of a stable flow increases with the depth of the lower layer. Simulations with a thick ($h_2/h_1=2$) and moderately thick ($h_2/h_1=0.87$) pycnocline show the same results.

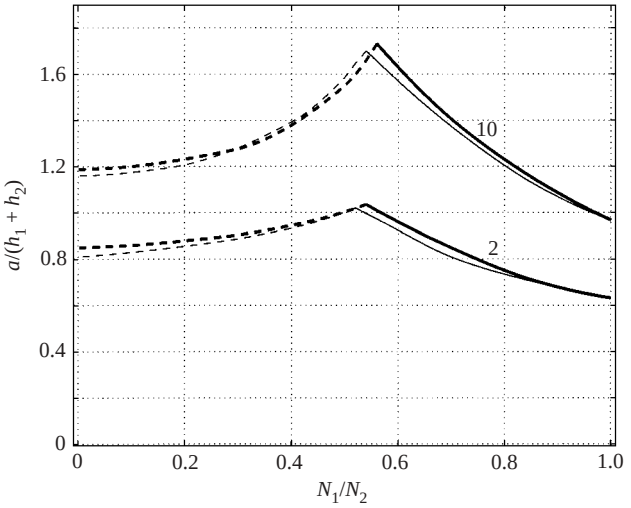

FIGURE 14. Maximum amplitude as a function of N_1/N_2. Dashed lines: $\omega/2\hat{N}=1$, solid lines: $u_{1max}/c=1$ for $h_3/(h_1+h_2)=2$ and 10. $h_2/h_1=2$ (thin lines) and $h_2/h_1=0.87$ (thick lines).

$a/(h_1+h_2)$	$a/(h_1+\frac{1}{2}h_2)$	h_2/h_1	$h_1+\frac{1}{2}h_2$	Obs.	Ref.
1.36	1.45	0.07	15 cm	Y	Case A
1.28	1.45	0.15	7.5 cm	N	Case B
1.41	1.5	0.07	15 cm	Y	Case C
1.27	1.35	0.07	15 cm	N	Fig. 2c
1.15	1.23	0.07	15 cm	N	Fig. 2c
0.85	0.91	0.07	15 cm	N	Fig. 2d

TABLE 1. Experimental observation of shear instability (Y)/no instability (N) by Grue *et al.* (1999). $N_1=0$, $N_2\neq 0$, $N_3=0$. In all cases $h_2=2$ cm and $(h_1+\frac{1}{2}h_2)/(h_3+\frac{1}{2}h_2)=4.13$.

5.4. *Comparison with experiments*

Grue *et al.* (1999) performed experiments on internal solitary waves of large amplitude propagating along a thin pycnocline. Experimental velocity and wave profiles were compared with fully nonlinear interfacial computations, with good agreement between experiment and theory. An aspect that was not explained was a breaking of the flow that took place within the pycnocline, in some of the runs with a very large amplitude. The breaking was clearly due to a shear instability. Two breaking cases were noted in Grue *et al.* (1999, § 4.1). The relative pycnocline thickness in most of the experiments was $h_2/h_1\simeq 0.07$. In one run it was $h_2/h_1\simeq 0.15$. The Brunt–Väisälä frequencies were $N_1=0$, $N_2\neq 0$, $N_3=0$. The data are reproduced in table 1 together with wave experiments where breaking was not observed. The observations are plotted together with the computations in figure 13(*a*). We observe that shear instability occurs for a significantly larger wave amplitude than indicated by a transition line corresponding to $Ri=1/4$. It is evident that instability occurs for a lower value of Ri than 1/4. Further precise experiments (and analysis) are required to invoke this transition.

Experimental observations of convective breaking, with $u/c\sim 1$, were made by Grue *et al.* (2000, § 7). Those experiments were performed with a stratified fluid with a shallow layer of linear stratification and a deep layer of constant density. In our

mathematical terminology the conditions were: $N_1/N_2 = 1$, $N_3 = 0$, $h_3/(h_1 + h_2) = 4.13$. Convective breaking was always observed when large waves induced a fluid velocity comparable to the wave speed. This occurred when the wave amplitude exceeded a certain value, i.e. $a/(h_1 + h_2) > 0.855$. Observations of convective breaking are indicated in figure 13 by the filled circles.

Convective breaking was also observed in the experiments by Grue *et al.* (2000) for waves with moderate amplitude, with u/c typically exceeding about 0.7. This breaking disappeared in the experiments when the free surface was covered by polystyrene, or when the stratified layer was below a homogeneous one, however. It was speculated that the reason for this latter type of breaking was due to the effect of capillarity at the free surface. Observations of such breaking are indicated by the filled squares in figure 13, and appear for values of u/c that are less than unity (and non-dimensional amplitudes less than 0.855). We note that the effect of capillarity, and other potential effects of a free surface that may trigger breaking of the waves, do not included in the present theory.

5.5. *Comments on waves with very large amplitude*

The limiting form of interfacial waves of very large amplitude was theoretically investigated by Pullin & Grimshaw (1988) and Rusås & Grue (2002), assuming homogeneous density in the layers. The conclusion from the latter reference is that interfacial waves of depression always tend to the conjugate flow limit (Amick & Turner 1986; Turner & Vanden-Broeck 1988), while waves of elevation grow in amplitude up to a limit that is smaller than the conjugate flow limit, and then have a mushroom-shaped overhanging profile, provided that the depth ratio is sufficiently large. These results are observed in computations with a finite density jump at the interface. In the Boussinesq limit, waves of depression and elevation have the same appearance, arriving at the conjugate flow limit when the wave amplitude becomes sufficiently large.

While no experimental mushroom-shaped waves of elevation have been observed, so far, the limiting form of interfacial waves of depression has partially been confirmed in experiments by Grue *et al.* (1999, figure 7*e*). The experimental profile at the front face of a wave generated by a very large initial disturbance compared exactly with fully nonlinear computations in the conjugate flow limit. A similar correspondence was observed for the measured wave phase velocity and the velocity profile induced by the wave. Breaking due to pronounced shear instability was observed in the pycnocline, at the rear of the wave. It can be concluded that the rear of the disturbance could not reach a steady form until the shear-induced breaking became less dominant or the wave amplitude was reduced. It is evident from the experiments by Grue *et al.* (1999) that (almost perfect) solitary waves can be generated until shear-induced breaking sets in.

5.6. *Computations of recirculation*

Solitary waves of mode one with trapped cores were experimentally observed by Grue *et al.* (2000). The trapped cores were characterized by intense breaking and by a horizontal fluid velocity that could only slightly exceed the wave velocity. In contrast to the experiments, the present calculation method predicts a region of recirculation when the wave amplitude is increased beyond the value when $u = c$ (see figure 15). The numerical results are obtained by giving a small increment in the wave speed, and finding the new field ψ. The computed results differ significantly from the experimental observations. The horizontal fluid velocity is not bounded by the wave

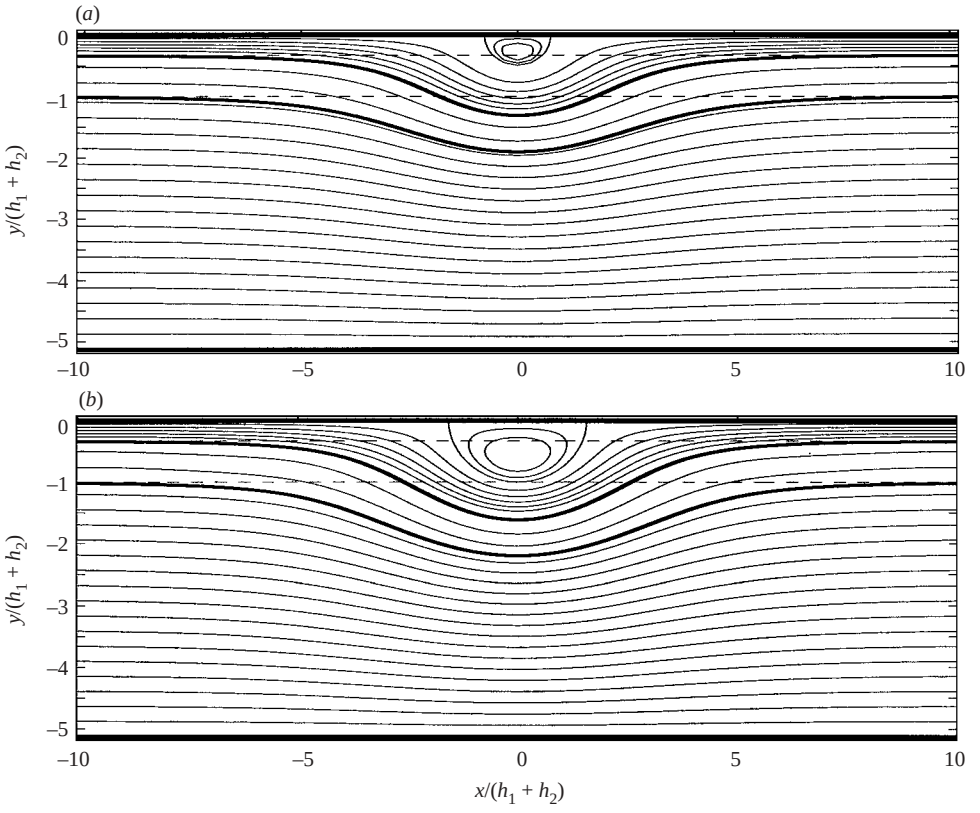

FIGURE 15. Streamlines for $a/(h_1+h_2)=0.90$ (a) and $a/(h_1+h_2)=1.20$ (b). $N_1/N_2=1$, $N_3=0$, $h_3/(h_1+h_2)=4.13$ and $h_2/h_1=2$.

speed, for example. Computations of large-amplitude solitary waves of mode one with regions of recirculation have been presented by several authors, see e.g. Tung *et al.* (1982) and Derzho & Grimshaw (1997). Recently, Lamb (2003) performed unsteady computations of solitary waves with trapped cores, with a fluid velocity that only slightly exceeded the wave velocity. A direct comparison between the experimentally observed velocity and vorticity fields in trapped cores and computations is yet to be done.

5.7. *Deflection of a free surface: estimate*

The deflection of the free surface, due to the passage of an internal wave, assuming that $\Delta\rho/\rho_0 \ll 1$, may be estimated by first computing the internal wave motion, assuming there is a rigid lid on the top of the fluid layer. The wave-induced increase in the pressure below the rigid lid is given by $\tilde{p}(x)-\tilde{p}_\infty=\frac{1}{2}(c^2-U^2(x))$, since the head $H=p+\rho g y+\frac{1}{2}\rho \boldsymbol{v}^2$ is constant along the streamline at $y=0$, where $\tilde{p}(x)$ and $\tilde{p}_\infty$ denote the pressure at $y=0$, at positions x and $x=\infty$, respectively, and $U(x)=\partial\Psi/\partial y$ at $y=0$. An estimate of the free-surface elevation relative to the elevation at infinity is obtained by equating $\rho g\tilde{\eta}(x)$ and $\tilde{p}(x)-\tilde{p}_\infty$, giving $\tilde{\eta}(x)=(1/2g)(c^2-U^2(x))$. A maximal elevation is obtained when $U(x)=c-u=0$ (the onset of convective breaking). (For $c\sim 1\,\mathrm{m\,s^{-1}}$ and $c=u$, the elevation $\tilde{\eta}$ becomes 5 cm at maximum.)

6. Conclusion

A fully nonlinear method to compute solitary waves propagating in a continuously stratified fluid has been derived. The stratification is represented by an arbitrary (finite) number of layers, each with a constant Brunt–Väisälä frequency. The method is a complement to two-layer interface models (Amick & Turner 1986; Turner & Vanden-Broeck 1988; Pullin & Grimshaw 1988; Evans & Ford 1996; Grue *et al.* 1999) and methods exploiting a continuously differentiable form of the stratification (Tung *et al.* 1982; Turkington *et al.* 1991).

The stream function satisfies the Helmholtz equation in each of the layers. This is expressed in terms of singularity distributions along the streamlines separating the layers. For the Green function a combination of Bessel functions of order zero, of the second and first kind is used, i.e. $Y_0(\hat{x}) + \alpha J_0(\hat{x})$, where α is a real constant. The set of singular integral equations is inverted by means of a Fourier transform. The resulting formulae show that the complementary spectra of $Y_0(\hat{x})$ and $J_0(\hat{x})$ are required to obtain good conditioning of the system of equations. This means that a non-zero value of α is advocated.

Computations are performed for two- and three-layer cases. The wave speed is found to increase with amplitude and increasing stratification in the top layer. The thickness of the pycnocline increases with amplitude when the layer above the pycnocline is homogeneous. The opposite is true when the top layer is stratified. The wave width exhibits a very small variation with the pycnocline thickness.

We have also investigated the effect of a stratified top layer on the wave-induced velocities and the kinematics within the pycnocline. The horizontal velocity generally increases with decreasing distance from the upper boundary when the stratification in the top layer is non-zero. The horizontal velocity relative to the wave speed first exceeds unity in the upper part of the water column. Convective breaking of experimental waves is thus expected to first occur close to the upper boundary of the fluid. This has been experimentally confirmed by Grue *et al.* (2000) for a two-layer fluid with a linearly stratified upper layer and a homogeneous lower layer. The fluid velocity is always smaller than the wave velocity in cases with a homogeneous layer at the top and bottom of the fluid. A convective breaking of the flow is then not expected.

The Richardson number is expressed by $Ri = (c^2 - cu)/N^2\delta^2$ where c denotes the wave speed, u the horizontal velocity, N the Brunt–Väisälä frequency of the isopycnal line in the far field and δ the vertical excursion of the isopycnal line. The main contribution to a small Ri is a large value of $|\delta|$. The minimal value of Ri is observed in the main body of the fluid, meaning that a shear instability is expected away from the horizontal boundaries.

Wave parameters with maximal u/c less than unity and minimal Ri greater than one quarter are expressed in terms of the wave amplitude and the characteristics of the stratification. The waves are expected to be non-breaking for $u/c < 1$ and $Ri > 1/4$. The computations may be used to calibrate experiments on breaking internal solitary waves, which is expected to take place for wave amplitudes that exceed the stable region indicated by theory. Further experimental investigations of convective breaking and shear instability caused by internal solitary waves should be undertaken. Breaking internal waves observed in the ocean, either in shoaling waters or at subsea ridges, do not yet have a satisfactory interpretation.

This work was funded by the Research Council of Norway through the BmatA-programme 'Computational methods for stratified flows involving internal waves' and

the Strategic University Programme 'General Analysis of Realistic Ocean Waves'. Partial funding was also received by the INTAS programme.

Appendix. Solution by Fourier transform

A Fourier transform of (3.8)–(3.13) gives $\mathscr{A}(k)X(k) = \mathscr{F}\{\mathscr{N}\mathscr{L}(X)\}(k)$ where $X^t = (\mathscr{F}\{\sigma_1\}, \mathscr{F}\{\sigma_2\}, \mathscr{F}\{\hat{\sigma_2}\}, \mathscr{F}\{\sigma_3\}, \mathscr{F}\{\eta\}, \mathscr{F}\{\hat{\eta}\})$, and

$$\mathscr{A}(k) = \begin{pmatrix} \beta_1^{(1)} - \beta_2^{(1)} & 0 & 0 & 0 & \mathrm{i}ck & 0 \\ \pi - \beta_3^{(1)} & \pi & \beta_3^{(2)} & 0 & 0 & 0 \\ 0 & \beta_1^{(2)} & \beta_2^{(2)} & 0 & \mathrm{i}ck & 0 \\ 0 & \beta_2^{(2)} & \beta_1^{(2)} & 0 & 0 & \mathrm{i}ck \\ 0 & \beta_3^{(2)} & \pi & \pi - \beta_3^{(3)} & 0 & 0 \\ 0 & 0 & 0 & \beta_1^{(3)} - \beta_2^{(3)} & 0 & \mathrm{i}ck \end{pmatrix} \tag{A 1}$$

where $\mathscr{F}\{f\}(k) = \int_{-\infty}^{\infty} f(x)\exp(-\mathrm{i}kx)\,\mathrm{d}x$. The system of equations is organized with the right-hand side $\mathscr{F}\{\mathscr{N}\mathscr{L}\}$ containing only nonlinear terms. The coefficients $\beta_i^{(j)}$, $i, j = 1, 2, 3$, result from the Fourier transform of the Green function involving $Z_1(\alpha, x) = Y_1(x) + \alpha J_1(x)$, i.e.

$$\beta_i^{(j)}(k) = \begin{cases} \beta_i^{(K_j, h_j, \alpha_j)} & \text{for } j = 2 \\ \beta_i^{(K_j, 2h_j, \alpha_j)} & \text{for } j = 1, 3, \end{cases} \tag{A 2}$$

$$\left.\begin{aligned} \beta_1^{(K,h,\alpha)}(k) &= \mathscr{F}\left\{\frac{\pi}{2}K\frac{Z_1(\alpha, K|u|)}{|u|}u\right\}(k), \\ \beta_2^{(K,h,\alpha)}(k) &= \mathscr{F}\left\{\frac{\pi}{2}K\frac{Z_1(\alpha, K\sqrt{u^2+h^2})}{\sqrt{u^2+h^2}}u\right\}(k), \\ \beta_3^{(K,h,\alpha)}(k) &= \mathscr{F}\left\{\frac{\pi}{2}Kh\frac{Z_1(\alpha, K\sqrt{u^2+h^2})}{\sqrt{u^2+h^2}}\right\}(k). \end{aligned}\right\} \tag{A 3}$$

By carrying out the transform we obtain

$$\beta_1^{(K,h,\alpha)}(k) = \begin{cases} \dfrac{-\alpha\mathrm{i}\pi k}{\sqrt{K^2-k^2}}, & |k| < K \\ \dfrac{\mathrm{i}\pi k}{\sqrt{k^2-K^2}}, & |k| > K, \end{cases} \tag{A 4}$$

$$\beta_2^{(K,h,\alpha)}(k) = \begin{cases} \dfrac{-\mathrm{i}\pi k[\sin(h\sqrt{K^2-k^2}) - \alpha\cos(h\sqrt{K^2-k^2})]}{\sqrt{K^2-k^2}}, & |k| < K \\ \mathrm{i}\pi\dfrac{k}{\sqrt{k^2-K^2}}\exp(-h\sqrt{k^2-K^2}), & |k| > K, \end{cases} \tag{A 5}$$

$$\beta_3^{(K,h,\alpha)}(k) = \begin{cases} -\pi\cos(h\sqrt{K^2-k^2}) + \alpha\pi\sin(h\sqrt{K^2-k^2}), & |k| < K \\ -\pi\exp(-h\sqrt{k^2-K^2}), & |k| > K. \end{cases} \tag{A 6}$$

A.1. *Discrete equations*

The system of equations $\mathscr{A}(k)X(k) = \mathscr{F}\{\mathscr{N}\mathscr{L}(X)\}(k)$ is solved for a prescribed wave celerity c. The relation between c and the wave amplitude a is subsequently computed. The wave amplitude is defined as the maximal negative displacement of the transition line $\hat{I}$ between the second and third layer, i.e $|\hat{\eta}(0)|$. A wave tank of length L is discretized with $n = 2^{\hat{n}}$ collocation points evenly spaced, $\hat{n}$ an integer. A corresponding set of wavenumbers are $k_j = 2\pi j/L$, $j = 1-n/2, \ldots, n/2$. The right-hand side of the discrete version of the equation involves all discrete wavenumbers, which means that the full block diagonal coefficient matrix has to be inverted. This matrix is denoted by $\boldsymbol{A}$.

The unknown functions σ_1, σ_2, $\hat{\sigma}_2$, σ_3, η and $\hat{\eta}$ are real and symmetric with respect to the vertical centreline of the wave at $x = 0$. Exploiting the symmetry, the resolution may be limited to the positive wavenumbers, leading to a system with $6n/2$ unknowns in the most general cases (b) and (c). In the far end of the wave tank we put the four unknown distributions and the two elevations are set to zero. This gives in the wavenumber space the following relations: $\mathscr{F}\{g\}(0) + 2\sum_{j=1}^{n/2} \mathscr{F}\{g\}(j)\cos(\mathrm{i}jL/2) = 0$, which are directly included in the global sparse matrix $\boldsymbol{A}$.

All the integrations are performed by the trapezoid rule. Derivatives are directly computed from their discrete Fourier transform. For practical computations we use $n = 128$ and $n = 256$. Convergence tests are run with $n = 512$. The tank length is chosen to be around ten times its height. An iterative scheme is used to find X for a prescribed celerity (initializing the procedure is explained below). The numbers of iterations needed to iterate the solution from c to $c + \Delta(c/c_0)c_0$ is typically around 20 for $\Delta(c/c_0) = 0.015$ with a maximum error $\epsilon = \sum_k |\mathscr{A}X - \mathscr{F}\{\mathscr{N}\mathscr{L}(X)\}| < 10^{-7}$.

A.2. *Resolution*

An iterative scheme is used to solve the set of discrete equations. Starting from a solution with a prescribed celerity c, the solution is found using the Newton–Raphson method. An initial guess X^0 is calculated from weakly nonlinear Korteweg–de Vries theory, giving $\sigma_1^0, \sigma_3^0, \eta^0, \hat{\eta}^0$, and from the set of equations, $\sigma_2^0, \hat{\sigma}_2^0$. The Jacobian matrix of the system is estimated by means of first-order finite difference. Its evaluation requires $7n$ nonlinear integral evaluations. The Jacobian is not re-computed at each step and its evaluation is done on a coarse grid with an adaptative step size.

A.3. *The condition number of the matrix* $\boldsymbol{A}$

We use the Green function $Z_0(\alpha, \hat{x}) = Y_0(\hat{x}) + \alpha J_0(\hat{x})$ where α is a (real) constant to be chosen. For the two-layer case (a) the Green function $Z_0(\alpha = 0, \hat{x}) = Y_0(\hat{x})$ was found to be satisfactory (Grue *et al.* 2000). An improved condition number of the set of equations is obtained here by a careful choice of a non-zero α, however. For the stratifications in cases (b) and (c), the matrix $\boldsymbol{A}$ becomes almost singular for values of α close to zero as indicated by a very small condition number of the matrix. The mathematical reason is that the function $\beta_1(k)^{(K,h,\alpha)}$ in (A 4) vanishes in the range $|k| < K$ when $\alpha = 0$. This means that the spectral components of the Green function become zero for $|k| < K$ when $\alpha = 0$. The condition number of the set of equations is improved with an α that is non-zero. In the computations we choose $\alpha = -1$ in the two-layer configuration and $\alpha = -1.2$ for the three-layer case. The computations for the case $N_1 = N_2$ confirm the computations by Grue *et al.* (2000), using another computational strategy with $\alpha = 0$, see figure 8.

REFERENCES

Amick, C. J. & Turner, R. E. L. 1986 A global theory of internal solitary waves in two-fluid systems. *Trans. Am. Math. Soc.* **298**, 431.

Bogucki, D. & Garrett, C. 1993 A simple model for the shear-induced decay of an internal solitary wave. *J. Phys. Oceanogr.* **23**, 1767.

Browand, F. K. & Wang, Y. H. 1972 An experiment on the growth of small disturbances at the interface between two streams of different densities and velocities. *Proc. Intl Symp. Stratified Flows, Aug 29–31, Novosibirsk, U.S.S.R.* ASCE.

Brown, D. J. & Christie, D. R. 1998 Fully nonlinear solitary waves in continuously stratified incompressible boussinesq fluids *Phys. Fluids* **10**, 2569.

Castro, I. P., Snyder, W. H. & Marsh, G. L. 1983 Stratified flow over three-dimensional ridges. *J. Fluid Mech.* **135**, 261.

Davies, R. E. & Acrivos, A. 1967 The stability of oscillatory internal waves. *J. Fluid Mech.* **30**, 723.

Delisi, D. P. & Orlanski, I. 1975 On the role of density jumps in the reflexion and breaking of internal gravity waves. *J. Fluid Mech.* **69**, 445.

Derzho, O. G. & Grimshaw, R. 1997 Solitary waves with a vortex core in a shallow layer of stratified fluid. *Phys. Fluids* **9**, 11.

Drazin, P. G. 1977 On the instability of and internal gravity wave. *Proc. R. Soc. Lond.* A **356**, 411.

Dubreil-Jacotin, L. 1932 Sur les ondes type permanent dans les liquides heterogenes. *Atti dela Reale Academic Nationale dci Lincei.* **15**(6), 44.

Eliassen, A. & Fjørtoft, R. 1992 The interface method for calculating the temporal evolution of a two-fluid system. *Frontiers of Science, Ann. NY Acad. Sci.* **661**, 54.

Evans, W. A. B. & Ford, M. J. 1996 An integral equation approach to internal (2-layer) solitary waves. *Phys. Fluids* **8**, 2032.

Grue, J., Friis, A., Palm, E. & Rusås, P.-O. 1997 A method for computing unsteady fully nonlinear interfacial waves. *J. Fluid Mech.* **351**, 223.

Grue, J., Jensen, A., Rusås, P.-O. & Sveen, J. K. 1999 Properties of large amplitude internal waves. *J. Fluid Mech.* **380**, 257.

Grue, J., Jensen, A., Rusås, P.-O. & Sveen, J. K. 2000 Breaking and broadening of internal solitary waves. *J. Fluid Mech.* **413**, 181.

Grue, J. & Ostrovsky, L. A. 2002 Analytical models and fully nonlinear computations of strongly nonlinear internal solitons. *Abstracts. European Geophy. Soc., Nice, April 2002.*

Hazel, P. 1972 Numerical studies of the stability of inviscid stratified shear flows. *J. Fluid Mech.* **51**, 39.

Holmboe, J. 1962 On the behaviour of symmetric waves in stratified shear layers. *Geophys. Publ.* (In memory of Vilhelm Bjerknes) **24**, 67.

Huthnance, J. M. 1989 Internal tides and waves near the continental shelf edge. *Geophys. Astrophys. Fluid Dyn.* **48**, 81.

Klostermeyer, J. 1982 On parametric instabilities of finite-amplitude internal gravity waves. *J. Fluid Mech.* **119**, 367.

Lamb, G. K. 1994 Numerical simulations of stratified inviscid flow over a smooth obstacle. *J. Fluid Mech.* **260**, 1.

Lamb, G. K. 2002 A numerical investigation of solitary internal waves with trapped cores formed via shoaling. *J. Fluid Mech.* **451**, 109.

Lamb, G. K. 2003 Shoaling solitary internal waves: on a criterion for the formation of waves with trapped core. *J. Fluid Mech.* **478**, 81.

Long, R. R. 1958 Tractable models of steady-state stratified flow with shear. *Q. J. R. Met. Soc.* **84**, 159.

Majda, A. J. & Shefter, M. G. 1998 Elementary stratified flows with instability at large Richardson number. *J. Fluid Mech.* **376**, 319.

McEvan, A. D. & Robinson, R. M. 1975 Parametric instability of internal gravity waves. *J. Fluid Mech.* **67**, 667.

Mied, R. P. 1976 The occurrence of parametric instabilities in finite-amplitude internal gravity waves. *J. Fluid Mech.* **78**, 763.

Orlanski, I. & Bryan, K. 1969 Formation of the thermocline step structure by large-amplitude internal gravity waves. *J. Geophys. Res.* **74**, 6975.

Ostrovsky, L. A. & Grue, J. 2003 Evolution equations for strongly nonlinear internal waves. *Phys. Fluids* **15**, 10.

Ostrovsky, L. A. & Stepanyants, Yu. A. 1989 Do internal solitons exist in the ocean? *Rev. Geophys.* **27**, 293.

Pelinovsky, E., Poloukhina, O. & Lamb, K. 2000 Nonlinear internal waves in the ocean stratified in density and flow. *Oceanology* **40**, N. 5, 805–815.

Pullin, D. I. & Grimshaw, R. H. J. 1988 Finite-amplitude solitary waves at the interface between two homogeneous fluids. *Phys. Fluids* **31**, 3550.

Rusås, P.-O. & Grue, J. 2002 Solitary waves and conjugate flows in a three-layer fluid. *Eur. J. Mech.* B/*Fluids* **21**, 185–206.

Scotti, R. S. & Corcos, G. M. 1972 An experiment on the stability of small disturbances in a stratified free shear layer. *J. Fluid Mech.* **52**, 499.

Stastna, M. & Lamb, K. G. 2002 Large fully nonlinear internal solitary waves: The effect of background current. *Phys. Fluids* **14**, 2987.

Stanton, T. P. & Ostrovsky, L. A. 1998 Observations of highly nonlinear internal solitons over the continental shelf. *Geophys. Rev. Lett.* **25**, 2695.

Tung, K.-K., Chan, T. F. & Kubota, T. 1982 Large amplitude internal waves of permanent form. *Stud. Appl. Maths* **66**, 1.

Turkington, B., Eydeland, A. & Wang, S. 1991 A computational method for solitary internal waves in a continuously stratified fluid. *Stud. Appl. Maths* **85**, 93.

Turner, R. E. L. & Vanden-Broeck, J.-M. 1988 Broadening of interfacial solitary waves. *Phys. Fluids* **31**, 2486.

Voronovich, A. G. 2003 Strong solitary internal waves in a 2.5-layer model. *J. Fluid Mech.* **474**, 85.

Winters, K. G. & D'Asaro, E. A. 1989 Two-dimensional instability of finite amplitude internal gravity wave packets near a critical level. *J. Geophys. Res.* **94**, 12709.

Yih, C.-S. 1960 Exact solutions for steady two-dimensional flow of a stratified fluid. *J. Fluid Mech.* **9**, 161.